

One-step synthesis of magnetic biosorbent for the removal of methylene blue

Dingning Chen^{a,c}, Jialei Chen^a, Zhiqiang Hu^a, Yan Zhu^b, Haoyu Shen^{a,*}

^aNingboTech University, Ningbo, Zhejiang 315100, China, emails: 21928125@zju.edu.cn (D. Chen), 2732548792@qq.com (J. Chen), 425009993@qq.com (Z. Hu), hyshe@nbt.edu.cn (H. Shen)

^bDepartment of Chemistry, Xixi Campus, Zhejiang University, Hangzhou 310028, China, email: zhuyan@zju.edu.cn

^cCollege of Chemical and Biological Engineering, Zhejiang University, Hangzhou 310028, China

Received 9 March 2021; Accepted 11 June 2021

ABSTRACT

In this paper, a facile co-precipitation method was used to prepare magnetic alkali-modified tea composites (MAT), and the low-cost adsorbent showed high adsorption performance for methylene blue (MB) in the aqueous solution. These adsorption experiments were carried out under different conditions, such as initial concentration, pH, MAT dosage, and temperature. The results showed that the adsorption capacity of MAT can reach 112.94 mg g⁻¹, which was higher than other biomaterials. The experiments of adsorption were designed by Design Expert Software and the optimal adsorption conditions were analyzed by ANOVA. The adsorption processes fitted the Langmuir isotherms well, and the pseudo-second-order equation was the best model to describe the adsorption behavior. It was potential material for the adsorption of MB.

Keywords: Waste tea; Fe₃O₄; Methylene blue; Adsorption; Response surface methodology

1. Introduction

The issue of dye pollution, mainly derived from textile, paper, plastic, food, cosmetics, and paint industries, must urgently be resolved and has aroused growing worldwide attention [1,2]. Methylene blue (MB) is one of the most widely used organic dyes, which is not only causing environmental pollution but also extremely harmful to human health due to its toxic, carcinogenic, and mutagenic properties, such as irritation of mouth, throat and stomach with symptoms of nausea and vomiting, diarrhea, delirium, and other symptoms.[3–5]. At present, various methods have been used to remove MB from wastewater, including adsorption separation [6,7], advanced oxidation process [8], membrane separation [9], and photolysis [10]. Among these operations, the adsorption method possesses a great promise for applications in wastewater treatment because of its ease of operation, simplicity of design, high efficiency,

low cost, and advantages in large-scale applications [11,12]. And many adsorbents with high adsorption capacities, including nanoporous carbon [13], organic-inorganic hybrid materials [14], and metal-organic frameworks [15], have been developed to deal with environmental pollution. However, the practical applications of adsorbents are greatly restricted due to their inherent defects, such as complex synthesis process and operation process, expensive cost, and nonbiodegradability [16,17]. It is necessary to develop high efficiency, low cost, and practical sorbents to tackle the above defects. Recently, natural biomass materials have attracted attention in wastewater treatment because of their low cost, sufficient sources, and biodegradability.

Tea waste (TW) is typical biomass, and its annual consumption is about 2 million tons in China [18]. TW can be prepared as a potential adsorbent for the removal of organic dyes in water treatments. In order to further improve the adsorption capacities of biomass, chemical-activation

* Corresponding author.

methods can be used to modify biomass to improve its surface area and pore structures. The activating chemical reagents include HCl, H_3PO_4 , NaOH, KOH, and metal salts [19]. Due to some inevitable defects of biomass materials, such as serious losses, few repetitions, and time-consuming, magnetic modified biomass materials present an innovative type of adsorption. The method contains a dispersion of the magnetic adsorbents into the sample solutions, and the separation was processed by the magnetic field. A critical step in this method is to simply separate the magnetic adsorbents from the solution without traditional filtration or centrifugation [20,21]. Thus, combining magnetic materials with TW can greatly simplify the operation steps.

Herein, this work reported a facile method to synthesize magnetic alkali-modified tea composites (MAT) by a one-step method. The removal efficiency of MB was evaluated by initial concentration, pH, MAT dosage, and temperature. Under the optimal experimental conditions, the adsorption processes fitted the pseudo-second-order and Langmuir isotherm well. The chemical component, structure, and morphology of MAT are systematically characterized with the Fourier transform spectroscopy (FTIR), scanning electron microscopy (SEM), transmission electron microscopy (TEM), X-ray photoelectron spectroscopy (XPS), X-ray diffraction (XRD), and Vibrating sample magnetometer (VSM).

2. Experiment

2.1. Materials

TW was purchased from a local market in Zhejiang, China. Other chemicals were analytical grade and purchased from the Sinopharm Chemical Reagent Co., Ltd., (Shanghai, China). All the dilutions were prepared with ultrapure water.

2.2. Preparation of MAT

TW was washed several times with boiled water and soaked in 0.1 mol L⁻¹ NaOH for 24 h. Then the alkali modified tea (AT) was washed by ultrapure water and dried.

MAT were prepared by a co-precipitation method. In brief, AT was dispersed into an aqueous solution containing 2.7 g FeSO₄·7H₂O and 3.5 g FeCl₃·6H₂O. Then, 10% NaOH was added slowly at 70°C until the pH reached 11. After the reaction, MAT was isolated under a magnetic field and washed with ultrapure water several times. Finally, MAT was dried in a vacuum oven at 60°C for 12 h.

2.3. Characterization

The structural, morphological, and physicochemical characteristics of the MAT were determined by different analytical methods including FTIR (Nexus 470), SEM (S-4800 Hitachi, Japan), TEM, XPS, XRD, and VSM (Lakeshore 7410).

2.4. Batch adsorption experiments

MB adsorption was measured through batch experiments in a series of 100 mL flasks. A certain amount of MAT was added to 25 mL of MB solution and shaken at 150 rpm. After adsorption, the residue of MB was measured by a UV-1700 spectrophotometer (Shimadzu, Japan)

at 664 nm. The experiments were performed under varying initial concentrations (20–400 mg L⁻¹), pH (2.0–10.0), temperature (30°C–50°C), and adsorbent dosages (0.01–0.10 g) regarding adsorption kinetics, adsorption isotherm, and thermodynamic study. All runs were repeated three times for greater accuracy. According to Eq. (1), the equilibrium adsorption capacity (mg g⁻¹) of MB was calculated.

$$q = \frac{(C_0 - C_e)V}{m} \quad (1)$$

where C_0 (mg L⁻¹) and C_e (mg L⁻¹) are the initial and the equilibrium concentrations of MB, respectively. And m (g) is the dosage of MAT, V (L) is the volume of solution.

The adsorption isotherm studies were investigated with MB initial concentration ranging from 20 to 400 mg L⁻¹. The Langmuir (Eq. (2)) and Freundlich (Eq. (3)) isotherm models were used for analyzing the data.

$$q_e = \frac{q_m K_L C_e}{1 + K_L C_e} \quad (2)$$

where q_m (mg g⁻¹) and K_L (L mg⁻¹) are the Langmuir constants related to the maximum adsorption capacity and apparent heat change, respectively:

$$q_e = K_F C_e^{1/n} \quad (3)$$

where K_F (mg g⁻¹)(dm³ mg⁻¹)^{1/n} is a Freundlich constant related to adsorption capacity and $1/n$ is a Freundlich constant related to the adsorption intensity.

The pseudo-first-order and pseudo-second-order models were used to describe the kinetics of the adsorption of MB by MAT, as listed in Eqs. (4) and (5).

$$q_e = q_m (1 - e^{-k_1 t}) \quad (4)$$

$$q_e = \frac{q_m^2 k_2 t}{1 + q_m k_2 t} \quad (5)$$

where q_m (mg g⁻¹) is the amount of dye adsorbed per unit weight of adsorbent at equilibrium, q_e (mg g⁻¹) is the amount of dye adsorbed at time t (min) and k_1 (min⁻¹), k_2 (g mg⁻¹ min⁻¹) are the rate constants.

The parameters (ΔH° , ΔS° , and ΔG°) of adsorption thermodynamics are calculated from the adsorption of MB on MAT at various temperatures by the following equations.

$$K_d = \frac{q_e}{C_e} \quad (6)$$

$$K_d = \exp\left(\frac{\Delta S^\circ}{R} - \left(\frac{\Delta H^\circ}{R}\right) \times \frac{1}{T}\right) \quad (7)$$

$$\Delta G^\circ = \Delta H^\circ - T\Delta S^\circ \quad (8)$$

where ΔH° and ΔS° are the enthalpy change (kJ mol⁻¹) and entropy change (J K⁻¹ mol⁻¹) during the adsorption process, and ΔG° is the Gibbs free energy change (kJ mol⁻¹). R is the

gas constant ($8.314 \text{ J mol}^{-1} \text{ K}^{-1}$). T is the absolute temperature (K), and K_d shows the adsorption distribution coefficient.

The pH_{pzc} defined as the pH for which the surface density of positive charges equals that of negative charges, was measured by the pH drift method [22]. In brief, 0.6 g MAT and 25 mL NaCl solution (0.01 M or 0.1 M) were shaken at 150 rpm for 2 h. The initial pH was adjusted by 0.1 M NaOH or 0.1 M HCl to range from 2 to 12. Then, the solutions were shaken again for 24 h, followed by final pH measurement (pH_f). The pH_{pzc} was obtained where pH_f was ~ 7 .

3. Results and discussion

3.1. Characterization

3.1.1. SEM and TEM analysis

The SEM and TEM are very useful techniques in providing the needed information about the size distribution and the morphology of synthesized adsorbent nanoparticles. As shown in Fig. 1a, MAT exhibited a rough surface with particles attached. The TEM image provides that the particles had nanostructure (Fig. 1b) and the dark areas were not evenly distributed on the appearance and in the pores. According to SEM-EDS (Fig. 1c), a large amount of Fe atom was found on MAT, which can demonstrate that Fe_3O_4 NPs have been successfully synthesized.

3.1.2. VSM analysis

The paramagnetic properties of MAT were quantified by the VSM. As Fig. 2a showed, the MAT exhibited the typical behavior of superparamagnetic materials and gives zero remanences, and the MS level of MAT was 14.70 emu g^{-1} . Its magnetic sensitivity was sufficient for its magnetic separation from the solution.

3.1.3. XPS analysis

The MAT composition was further verified through the XPS. From Fig. 2b, four peaks originated from Fe, O, N, and C elements, respectively, revealing the co-existence of these elements in the MAT. Fig. 2c showed the XPS high-resolution spectra from 740 to 702.5 eV which contained two well-defined peaks at 725.3 and 711.7 eV

correspond to Fe 2p_{1/2} and Fe 2p_{3/2} in Fe_3O_4 . Fig. 2d showed the C 1s spectrum that can be divided into three components: (1) C=C (284.8 eV), (2) C–O (286.1 eV), and (3) N–C=O (288.0 eV) [23]. Based on an earlier study [24], the presence of N–C=O groups was of significance to anchor Fe_3O_4 via the reaction of amino groups with iron ions.

3.1.4. XRD analysis

Fig. S1 shows the XRD pattern of MAT. The diffraction peaks at 30.1° , 35.5° , 43.1° , 53.6° , 57.1° , and 62.6° corresponded to (220), (311), (400), (511), and (440). These peaks matched well with the standard PDF cards (99-0073).

3.1.5. FTIR analysis

As seen in Fig. S2, the FTIR spectrum of MAT showed the broad and strong band at 3400 cm^{-1} because of the stretching vibrations of O–H. And the peak at $1,637 \text{ cm}^{-1}$ was assigned to the stretching vibration of the aromatic ring and vibration of N–H [12]. The peaks of $1,544$ and $1,066 \text{ cm}^{-1}$ belonged to the N–H shearing vibration of the amide group and the vibration of the C–O. The peak at 580 cm^{-1} belonged to the Fe–O bond vibration of Fe_3O_4 .

3.2. Effect of operating conditions on MB adsorption

3.2.1. Effect of solution pH

The effect of the initial solution pH on the removal of MB was analyzed over the pH range from 2.0 to 12.0. And the pH was adjusted by 0.01 mol L^{-1} NaOH and 0.01 mol L^{-1} HCl solution. MB existed in the aqueous solution in the form of positively charged ions [25]. The knowledge of pH_{pzc} allows one to hypothesize on the ionization of functional groups and their interaction with species in solution; at solution pHs higher than pH_{pzc} sorbent surface is negatively charged and could interact with positive species while at pHs lower than pH_{pzc} solid surface is positively charged and could interact with negative species. From Fig. 3a, the results showed that the pH_{pzc} was ~ 7.06 . The adsorption capacity of MB increased significantly with increasing the solution pH from 2 to 4 ($\text{pHs} < \text{pH}_{\text{pzc}}$). When the pH was below 4, MAT may acquire a positive surface charge because of the protonation of the amino

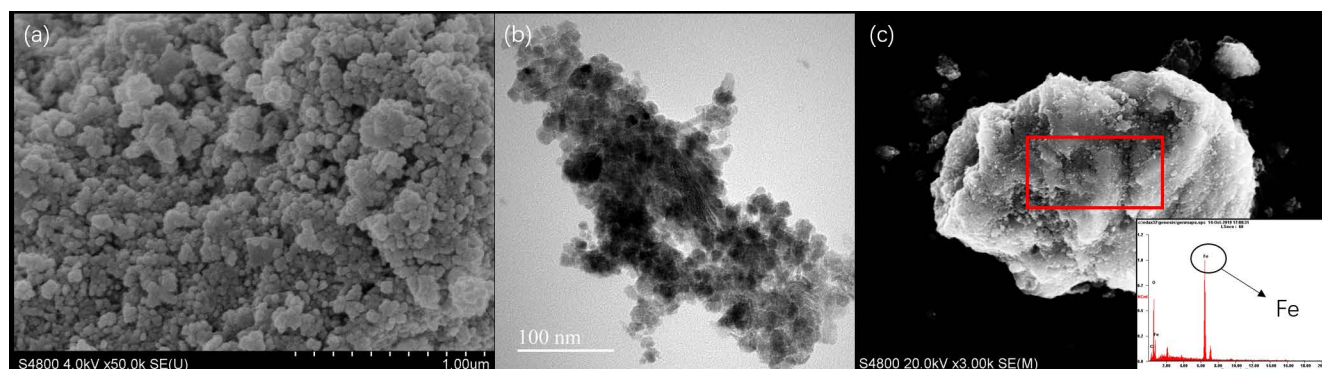


Fig. 1. (a) SEM, (b) TEM, and (c) SEM-EDS images of MAT.

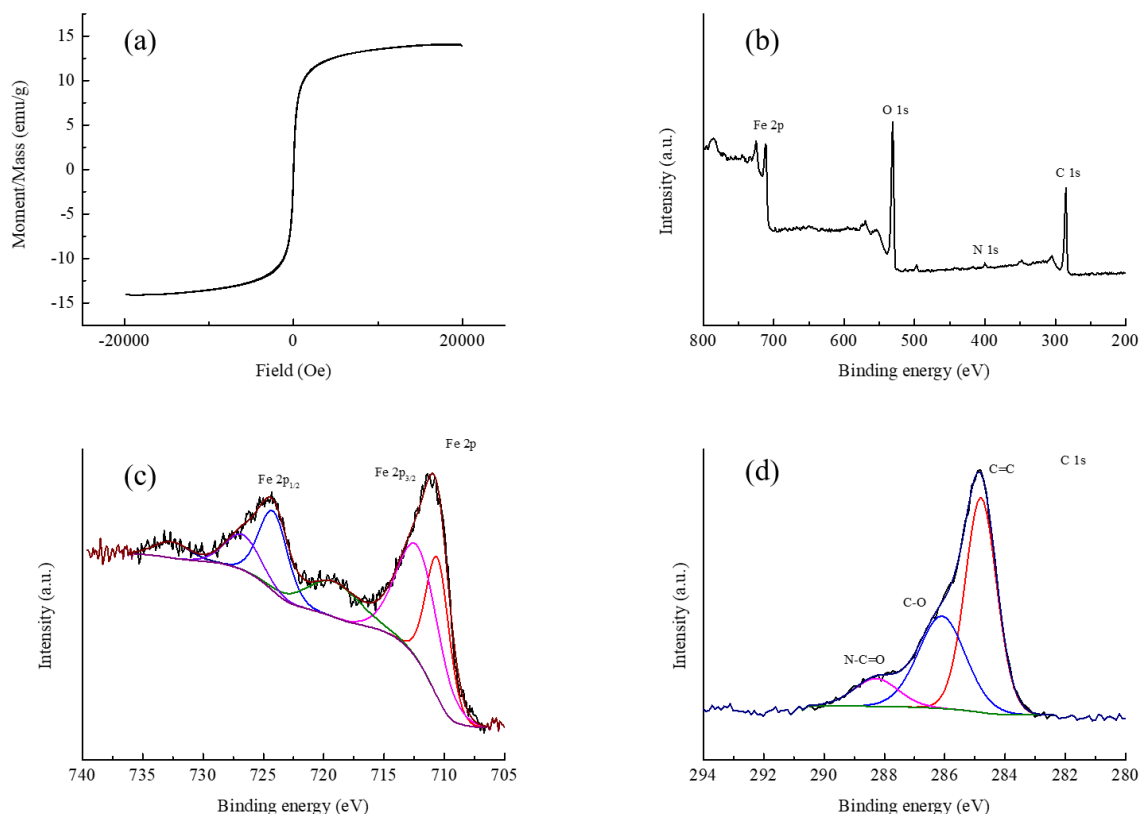


Fig. 2. VSM and XPS characterization of MAT: (a) VSM, (b) Survey, (c) Fe 2p, and (d) C1s.

groups, and electrostatic repulsion (main interaction) between MAT and MB occurred resulting in the low adsorption capacity. However, when the pH value was 2, the q_e can still reach 29.95 mg g^{-1} . The reason may be attributed to the π -stacking and hydrogen bonding between adsorbent and adsorbate, as there were abundant aromatic rings and phenolic groups on MAT composites. When the pH is in the range of 4 to 10, the main interactions of adsorption were π -stacking and hydrogen bonding. When pH was higher than 10, the surface charge of the composites became negative because of the deprotonation of the phenolic groups, and the adsorption capacity will also get a significant improvement due to electrostatic interaction. However, the condition of $\text{pH} > 10$ was not used as reference data for the following experiments because the magnetic beads cannot exist stably under strong alkaline solutions.

3.2.2. Effect of adsorbent dosage

The adsorbent dosage may affect the number of adsorption sites and thereby affected the adsorption behaviors. Fig. 3b exhibits the adsorption percentage of MB on the variation of MAT dosage. It can be observed that the adsorption percentage increased with an increasing adsorbent dosage. The reason was that there were more available adsorption surfaces and sites by adding MAT.

Fig. 3c shows that different initial concentrations on the adsorption of MB. The q_e (mg g^{-1}) at equilibrium increased from 25.0 to 111.1 mg g^{-1} as the initial concentration was

increased from 20 to 400 mg L^{-1} . The increasing of initial concentration can improve the driving force to overcome the mass transfer resistances of MB between the aqueous and solid phases. Hence, a suitable initial concentration will promote the adsorption process. In general, the optimum MAT dosage and initial concentration were found to be 0.60 g and 200 mg L^{-1} .

3.2.3. RSM analysis of adsorption

Experiments of removal of MB were designed by the Design Expert Software. Different adsorbent dosages (A), initial concentrations (B), and pH (C) were given by experimental design and the q_e was selected as the response (Table S1). All experimental runs are shown in Table S2. The results were analyzed by ANOVA (Tables S3 and S4) and a mathematical model was formed by Design Expert 8.0.6 Trial Program. The fitted equation was presented as 3D surface plots to visualize the relationship of experimental factors and responses.

The p -value was used to evaluate the significance of each term by using statistical analysis. The p -value of each term was determined and the impact that gives a p -value < 0.05 is determined as significant. The ANOVA analysis for the proposed model of adsorption was presented in Tables S3 and S4. The achieved regression equation of the ANOVA showed that the correlation (R^2) for the adsorption capacity was 0.9929. And the prediction R^2 of 0.9683 was in reasonable agreement with the adjusted

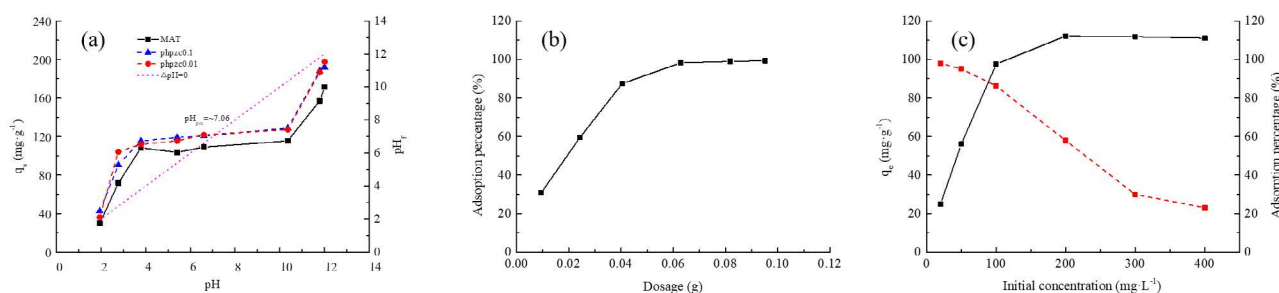


Fig. 3. Effect of (a) pH, (b) adsorbent dosage, and (c) initial concentration on the adsorption of MB on MAT.

R^2 of 0.9886. These results showed that the correlation between empirical and the calculated values were acceptable. Although the adsorption capacity with a p -value of 0.087 means lack of fit, the quadratic model is also reliable for the current research. Therefore, the high R^2 -value, remarkable F -value (231.69), insignificant P -value, and low PRESS (66.62) illustrate the high dependability of the models in predicting the responses. The equation connecting the q_e -value to coded factors are shown as Eq. (9):

$$q_e = 82.38 - 14.35 \times A + 7.20 \times B + 0.77 \times C - 2.24 \times A \times B - 0.25 \times A \times C - 0.16 \times B \times C \quad (9)$$

where A , B , and C were adsorbent dose, initial concentration, and pH, respectively.

Based on these results, several response surface plots of MAT adsorption capacity can be obtained, as shown in Fig. 4. From Table S3, only AB was significant of all the interaction terms (Fig. 4a). According to these results, it determined that the adsorbent dose and initial concentration were important for the removal of MB by MAT, when the pH was higher than 4. Between 0.50–0.70 g of adsorbent dose and 180–220 mg L⁻¹ of initial concentration, a plateau of q will appear which was in agreement with Fig. 3b and c. And from Fig. 4, the interaction terms of AC and BC were not significant. But the change of adsorption amount was very small which was in agreement with Fig. 3a, when $pH > 4$.

3.3. Isotherm analysis

There were several equilibrium models, which have been used to describe the adsorption isotherm relationship. The applicability of the isotherm models to the adsorption study was judged by the correlation coefficient. Comparing Langmuir ($R^2 = 0.9890$) and Freundlich ($R^2 = 0.8152$) models, it was found that the R^2 of Langmuir isotherm was higher (Fig. 5).

According to Langmuir isotherm, the process was monolayer adsorption. The maximum sorption capacity (q_m , 112.94 mg g⁻¹) can be calculated from Eq. (2), and K_L was found to be 0.47. And it can be observed that the adsorption capacity of MAT was higher than others (Table 1).

3.4. Adsorption kinetics and thermodynamic parameters

In order to examine the rate of the adsorption process by kinetic models. In the present work, the pseudo-first-order

(Eq. (4)) and pseudo-second-order (Eq. (5)) were used to analyze the batch studies. Results showed that the pseudo-second-order model ($R^2 = 0.9951$, $k_2 = 0.0118$ g mg⁻¹ min⁻¹) provided a better correlation than the pseudo-first-order model ($R^2 = 0.9818$, $k_1 = 0.8183$ min⁻¹). Thus, there may be chemical adsorption in the adsorption process.

In addition, between the relationship of K_d and T , a non-linear plot can be obtained, as shown in Fig. S3b. ΔH° , ΔS° and ΔG° were calculated by Eqs. (6)–(8) (Table 2). Adsorption of MB was measured at optimal conditions at three temperatures of 303, 318, 323 K. The results showed that the capacity of MB adsorption decreased with increasing temperature because increasing the temperature inhibited the progress of the exothermic reaction. The negative Gibbs free energy changes indicate the spontaneity of MB adsorption by MAT. Moreover, the negative value of entropy changes suggested decreased disorder in the solid-solution interface during adsorption.

3.5. Adsorption mechanisms

Firstly, it can be observed that there are amino and phenolic hydroxyl groups on MAT from the XPS and FTIR. The results of pH experiments show that the adsorption capacity onto MAT increases significantly with increasing pH. According to kinetic data, the adsorption behavior of MB on MAT is more consistent with chemical adsorption. These phenomena suggest that there is electrostatic interaction in the adsorption process. Secondly, when the pH value is 2, the q_e can still reach 29.95 mg g⁻¹. It may involve hydrogen bond and π -stacking because of hydroxyl and aromatic ring groups on MAT. The possible adsorption mechanism, including electrostatic interaction, hydrogen bond, and π -stacking, was schematically illustrated in Fig. 6.

3.6. Real samples and stability analysis

The selective adsorption of MB by MAT in practical applications was studied by using laboratory wastewater. The wastewater containing 200 mg L⁻¹ MB, NaCl (0–50 mg L⁻¹), and rhodamine B (0–50 mg L⁻¹) was adjusted to optimal conditions. 0.6 g of adsorbent and 25 mL of wastewater solution were put into a 50 mL centrifuge tube and react at room temperature for 2 h, then separate the solid and liquid. A UV detector was used to determine the MB concentration before and after adsorption. Fig. 7a shows the adsorption results of MAT for MB

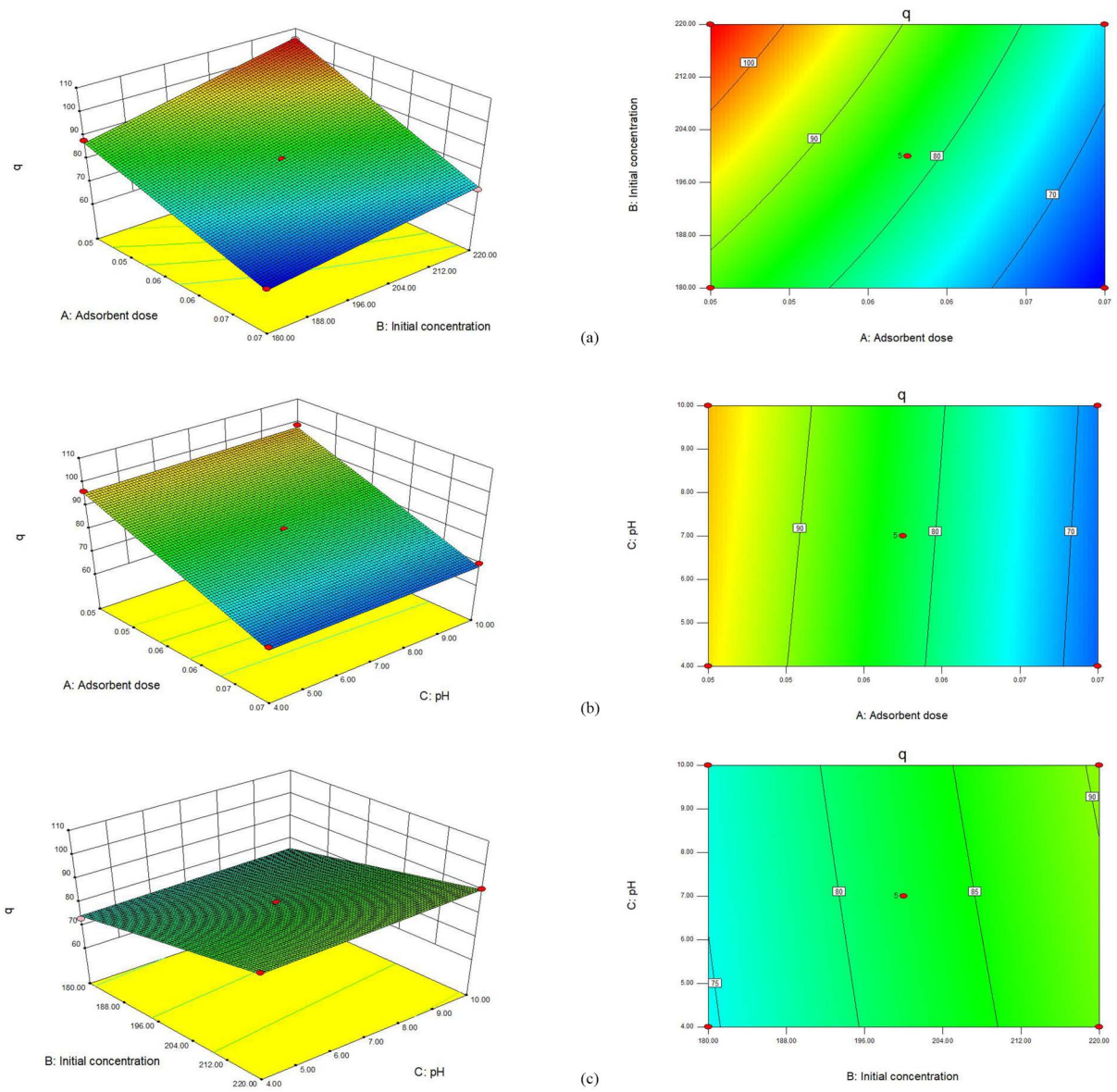


Fig. 4. Response surface plots of MAT adsorption capacity: (a) effect of adsorbent dose versus initial concentration, (b) effect of adsorbent dose versus pH, and (c) effect of initial concentration versus pH.

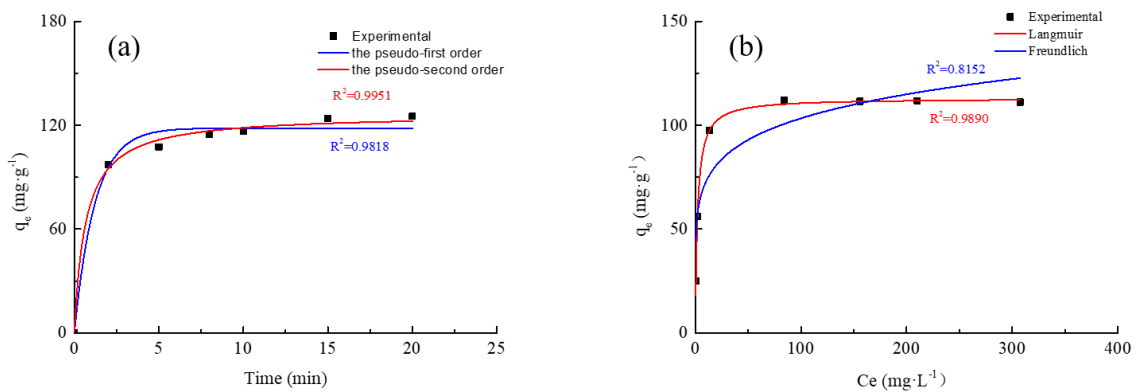


Fig. 5. (a) Kinetics and (b) isotherm models of the adsorption of MB on MAT.

in wastewater, indicating that MAT has a poor adsorption effect on complex wastewater. The stability of the adsorbent was studied by repeated adsorption–desorption experiments under optimal conditions. After desorption, MAT was regenerated in 0.1 M HCl solution at 30°C for 0.5 h. As shown in Fig. 7b, the MAT composites can be used at least five times with acceptable reproducibility and repeatability.

Table 1
Adsorbents comparative study of MB adsorption

Adsorbent	Adsorption capacity (mg g ⁻¹)	Reference
Lotus leaf	221.7	[26]
Waste tea	85.5	[27]
Garlic peel	82.6	[28]
Acid-treated pyrolytic tire char	65.8	[29]
Carbon nanotubes	64.7	[30]
Wheat straw biochar powder	62.5	[31]
<i>Cortaderia selloana</i> flower spikes	47.9	[32]
Freeze-dried agarose gel	10.4	[33]
Defatted algal biomass	7.73	[34]
MAT	112.9	This work

4. Conclusions

The results demonstrated that the AT can be used for the removal of MB from its aqueous solutions. And the modified tea was decorated with magnetic nanoparticles so that it can accelerate separation efficiency by magnetic fields. Compare the Langmuir to Freundlich models, Langmuir can better describe the adsorption behavior of MB on MAT, and also shows that the adsorption behavior of MB on MAT is single-layer adsorption. At the same time, the theoretical adsorption capacity obtained by the Langmuir model ($q_e = 112.94 \text{ mg g}^{-1}$) is closer to the adsorption capacity obtained from the experiment ($q_e = 111.12 \text{ mg g}^{-1}$). The adsorption process conforms to the pseudo-second-order model. The removal efficiency increases with the increase in pH at 2–4. The MAT not only

Table 2
Thermodynamic parameters for the adsorption of MB on MAT

T (K)	ΔG° (kJ mol ⁻¹)	ΔH° (kJ mol ⁻¹)	ΔS° (J mol ⁻¹ K ⁻¹)
303	-1.19	-17.92	-55.20
318	-0.37		
323	-0.09		

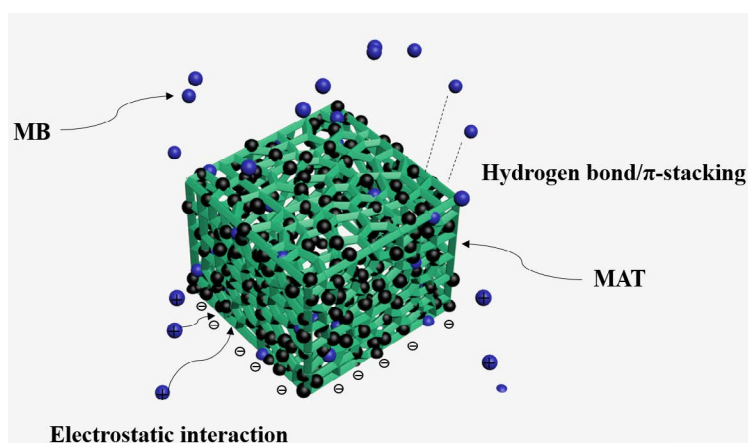


Fig. 6. Schematic illustration of MB adsorption on MAT.

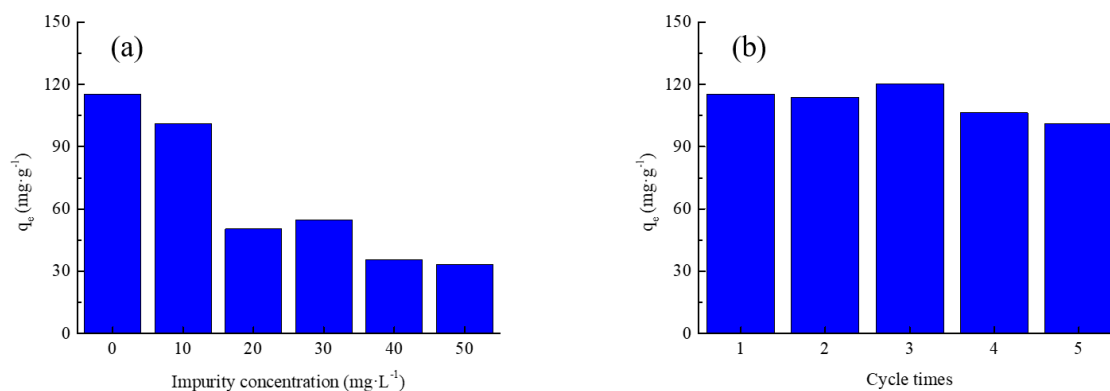


Fig. 7. (a) Real samples and (b) stability analysis of MAT.

has higher adsorption but also has shown additional benefits like environmental-friendliness, low cost, and low toxicity. Therefore, the adsorbent is expected to be a promising advanced adsorbent.

Acknowledgements

This work was performed under the financial support of the Natural Science Foundation of China (No. 51608479), the Natural Science Foundation of Zhejiang Province (No. LGC20B070001), the Innovation Planning Project of Ningbo (No. 2019CXGC006) and the Zhejiang Provincial Department of Science and Technology is acknowledged for this research under its Provincial Key Laboratory Programme (No. 2020E10018).

References

- H.N. Tran, S.J. You, A. Hosseini-Bandegharai, H.P. Chao, Mistakes and inconsistencies regarding adsorption of contaminants from aqueous solutions: a critical review, *Water Res.*, 120 (2017) 88–116.
- G. Zhang, X. Zhang, Y. Meng, G. Pan, Z. Ni, S. Xia, Layered double hydroxides-based photocatalysts and visible-light driven photodegradation of organic pollutants: a review, *Chem. Eng. J.*, 392 (2020) 123684, doi: 10.1016/j.cej.2019.123684.
- C. Duan, X. Meng, C. Liu, W. Lu, J. Liu, L. Dai, W. Wang, W. Zhao, C. Xiong, Y. Ni, Carbohydrates-rich corn cobs supported metal-organic frameworks as versatile biosorbents for dye removal and microbial inactivation, *Carbohydr. Polym.*, 222 (2019) 115042, doi: 10.1016/j.carbpol.2019.115042.
- S. Soni, P.K. Bajpai, J. Mittal, C. Arora, Utilisation of cobalt doped iron based MOF for enhanced removal and recovery of methylene blue dye from waste water, *J. Mol. Liq.*, 314 (2020) 113642, doi: 10.1016/j.molliq.2020.113642.
- J. Mittal, Permissible synthetic food dyes in India, *Reson. J. Sci. Educ.*, 25 (2020) 567–577.
- Q. Liu, H. Yu, F. Zeng, X. Li, J. Sun, C. Li, H. Lin, Z. Su, HKUST-1 modified ultrastability cellulose/chitosan composite aerogel for highly efficient removal of methylene blue, *Carbohydr. Polym.*, 255 (2021) 117402, doi: 10.1016/j.carbpol.2020.117402.
- E. Özmetin, M.M. Kocakerim, Removal of methylene blue dye from aqueous solutions by illite clay, *Desal. Water Treat.*, 124 (2018) 279–286.
- I. Oller, S. Malato, J.A. Sanchez-Perez, Combination of advanced oxidation processes and biological treatments for wastewater decontamination – a review, *Sci. Total Environ.*, 409 (2011) 4141–4166.
- Y. Ding, J. Wu, J. Wang, J. Wang, J. Ye, F. Liu, Superhydrophilic carbonaceous-silver nanofibrous membrane for complex oil/water separation and removal of heavy metal ions, organic dyes and bacteria, *J. Membr. Sci.*, 614 (2020) 118491, doi: 10.1016/j.memsci.2020.118491.
- K.L. Jia, Z.S. Zhu, J. Qu, Y.Q. Jing, X.J. Yu, Y. Abdelkrim, S.M. Hao, Z.Z. Yu, BiOBr/Ag₆Si₂O₇ heterojunctions for enhancing visible light catalytic degradation performances with a sequential selectivity enabled by dual synergistic effects, *J. Colloid. Interface Sci.*, 561 (2020) 396–407.
- J.C. Zuo, S.R. Tong, X.L. Yu, L.Y. Wu, C.Y. Cao, M.F. Ge, W.G. Song, Fe³⁺ and amino functioned mesoporous silica: preparation, structural analysis and arsenic adsorption, *J. Hazard. Mater.*, 235–236 (2012) 336–342.
- J. Fu, Z. Chen, M. Wang, S. Liu, J. Zhang, J. Zhang, R. Han, Q. Xu, Adsorption of methylene blue by a high-efficiency adsorbent (polydopamine microspheres): kinetics, isotherm, thermodynamics and mechanism analysis, *Chem. Eng. J.*, 259 (2015) 53–61.
- W. Wang, T. Lu, Y. Chen, G. Tian, V.K. Sharma, Y. Zhu, L. Zong, A. Wang, Mesoporous silicate/carbon composites derived from dye-loaded palygorskite clay waste for efficient removal of organic contaminants, *Sci. Total Environ.*, 696 (2019) 133955, doi: 10.1016/j.scitotenv.2019.133955.
- F.Y. Yi, W. Zhu, S. Dang, J.P. Li, D. Wu, Y.H. Li, Z.M. Sun, Polyoxometalates-based heterometallic organic-inorganic hybrid materials for rapid adsorption and selective separation of methylene blue from aqueous solutions, *Chem. Commun. (Camb)*, 51 (2015) 3336–3339.
- Q. Yang, S. Ren, Q. Zhao, R. Lu, C. Hang, Z. Chen, H. Zheng, Selective separation of methyl orange from water using magnetic ZIF-67 composites, *Chem. Eng. J.*, 333 (2018) 49–57.
- Q. Liu, S. Li, H. Yu, F. Zeng, X. Li, Z. Su, Covalently crosslinked zirconium-based metal-organic framework aerogel monolith with ultralow-density and highly efficient Pb(II) removal, *J. Colloid. Interface Sci.*, 561 (2020) 211–219.
- Q. Liu, H. Yu, F. Zeng, X. Li, J. Sun, X. Hu, Q. Pan, C. Li, H. Lin, Z. Min Su, Polyaniline as interface layers promoting the in-situ growth of zeolite imidazole skeleton on regenerated cellulose aerogel for efficient removal of tetracycline, *J. Colloid. Interface Sci.*, 579 (2020) 119–127.
- Q. Xu, K. Hu, X. Wang, D. Wang, M.T. Knudsen, Carbon footprint and primary energy demand of organic tea in China using a life cycle assessment approach, *J. Cleaner Prod.*, 233 (2019) 782–792.
- B. Li, Y. Zhang, J. Xu, Y. Mei, S. Fan, H. Xu, Effect of carbonization methods on the properties of tea waste biochars and their application in tetracycline removal from aqueous solutions, *Chemosphere*, 267 (2021) 129283, doi: 10.1016/j.chemosphere.2020.129283.
- A. Khoobi, M. Salavati-Niasari, O. Amiri, Ultrasonic synthesis and characterization of SnFe₁₂O₁₉/GO nanocomposite: application of multivariate optimization in magnetic solid-phase extraction, *J. Alloys Compd.*, 858 (2021) 157745, doi: 10.1016/j.jallcom.2020.157745.
- N. Li, H.-L. Jiang, X. Wang, X. Wang, G. Xu, B. Zhang, L. Wang, R.-S. Zhao, J.-M. Lin, Recent advances in graphene-based magnetic composites for magnetic solid-phase extraction, *TrAC Trends Anal. Chem.*, 102 (2018) 60–74.
- X. Yu, J. Zhang, Y. Zheng, Perchlorate adsorption onto epichlorohydrin crosslinked chitosan hydrogel beads, *Sci. Total Environ.*, 761 (2021) 143236, doi: 10.1016/j.scitotenv.2020.143236.
- S. Yang, N. Okada, M. Nagatsu, The highly effective removal of Cs⁺ by low turbidity chitosan-grafted magnetic bentonite, *J. Hazard. Mater.*, 301 (2016) 8–16.
- T. Wen, J. Wang, X. Li, S. Huang, Z. Chen, S. Wang, T. Hayat, A. Alsaedi, X. Wang, Production of a generic magnetic Fe₃O₄ nanoparticles decorated tea waste composites for highly efficient sorption of Cu(II) and Zn(II), *J. Environ. Chem. Eng.*, 5 (2017) 3656–3666.
- J. Zhang, S. Chen, H. Zhang, X. Wang, Removal behaviors and mechanisms of hexavalent chromium from aqueous solution by cephalosporin residue and derived chars, *Bioresour. Technol.*, 238 (2017) 484–491.
- X. Han, W. Wang, X. Ma, Adsorption characteristics of methylene blue onto low cost biomass material lotus leaf, *Chem. Eng. J.*, 171 (2011) 1–8.
- M.T. Uddin, M.A. Islam, S. Mahmud, M. Rukanuzzaman, Adsorptive removal of methylene blue by tea waste, *J. Hazard. Mater.*, 164 (2009) 53–60.
- B.H. Hameed, A.A. Ahmad, Batch adsorption of methylene blue from aqueous solution by garlic peel, an agricultural waste biomass, *J. Hazard. Mater.*, 164 (2009) 870–875.
- V. Makrigianni, A. Giannakas, Y. Deligiannakis, I. Konstantinou, Adsorption of phenol and methylene blue from aqueous solutions by pyrolytic tire char: equilibrium and kinetic studies, *J. Environ. Chem. Eng.*, 3 (2015) 574–582.
- Y. Yao, F. Xu, M. Chen, Z. Xu, Z. Zhu, Adsorption behavior of methylene blue on carbon nanotubes, *Bioresour. Technol.*, 101 (2010) 3040–3046.
- G. Li, W. Zhu, C. Zhang, S. Zhang, L. Liu, L. Zhu, W. Zhao, Effect of a magnetic field on the adsorptive removal of methylene blue onto wheat straw biochar, *Bioresour. Technol.*, 206 (2016) 16–22.
- N. Mechi, I. Ben Khemis, G.L. Dotto, D. Franco, L. Sellaoui, A. Ben Lamine, Investigation of the adsorption mechanism of methylene blue (MB) on *Cortaderia selloana* flower spikes (FSs) and on *Cortaderia selloana* flower spikes derived carbon fibers (CFs), *J. Mol. Liq.*, 280 (2019) 268–273.
- W.Y. Seow, C.A.E. Hauser, Freeze-dried agarose gels: a cheap, simple and recyclable adsorbent for the purification of

methylene blue from industrial wastewater, *J. Environ. Chem. Eng.*, 4 (2016) 1714–1721.

[34] T.S. Chandra, S.N. Mudliar, S. Vidyashankar, S. Mukherji, R. Sarada, K. Krishnamurthi, V.S. Chauhan, Defatted algal

biomass as a non-conventional low-cost adsorbent: surface characterization and methylene blue adsorption characteristics, *Bioresour. Technol.*, 184 (2015) 395–404.

Supplementary information

Table S1

Variables used in the full factorial design with coded and actual values

Factor	Units	Coded and actual levels		
		Low (−1)	Medium (0)	High (+1)
Adsorbent dose (A)	g	0.05	0.06	0.07
Initial concentration (B)	mg L ^{−1}	180	200	220
pH (C)	–	4	7	10

Table S2

Experimental design and results by using RSM

Run	A	B	C	q_e (mg g ^{−1})
1	−1	0	+1	98.72
2	0	0	0	82.22
3	0	+1	−1	89.14
4	0	0	0	82.74
5	0	0	0	82.58
6	+1	0	−1	68.64
7	0	−1	+1	74.24
8	+1	+1	0	71.81
9	0	−1	−1	73.28
10	0	0	0	81.28
11	0	0	0	81.27
12	−1	0	−1	96.43
13	+1	−1	0	63.67
14	+1	0	+1	69.94
15	0	+1	+1	90.74
16	−1	+1	0	105.42
17	−1	−1	0	88.31

Table S3

Results of ANOVA for RSM model (1)

Source	Sum of squares	df	Mean square	F-value	p-value Probe > F	Remarks
Model	2,088.01	6	348.00	231.69	<0.0001	Significant
A	1,647.95	1	1,647.95	1,097.15	<0.0001	
B	414.86	1	414.86	276.20	<0.0001	
C	4.73	1	4.73	3.15	0.1064	
AB	20.12	1	20.12	13.39	0.0044	
AC	0.25	1	0.25	0.16	0.6948	
BC	0.10	1	0.10	0.068	0.7993	
Residual	15.02	10	1.50			
Lack of fit	13.04	6	2.17	4.39	0.0870	Insignificant
Pure error	1.98	4	0.50			
Cor. total	2,103.03	16				

Table S4
Results of ANOVA for RSM model (2)

Std. Dev	1.23	R-Square	0.9929
Mean	82.38	Adj. R-Square	0.9886
C.V. %	1.49	Pred. R-Square	0.9683
PRESS	66.62	Adeq. Precision	54.814

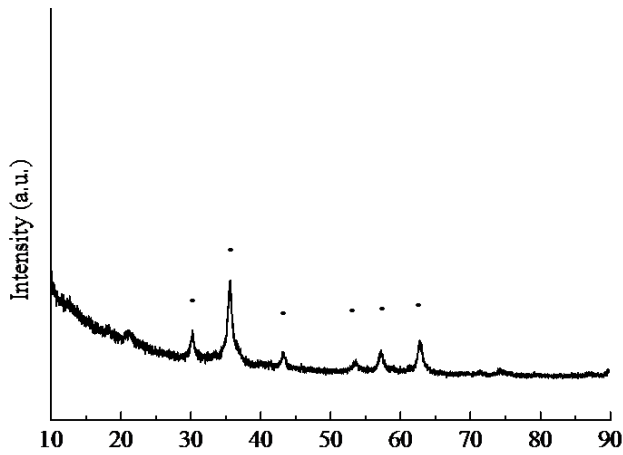


Fig. S1. XRD analysis of the MAT.

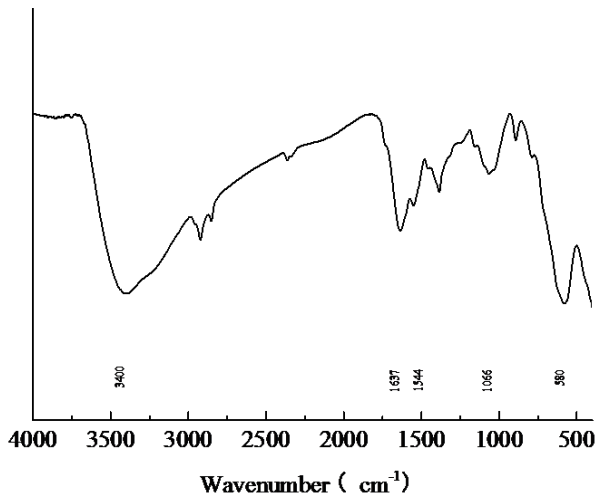


Fig. S2. FTIR spectrum of MAT.

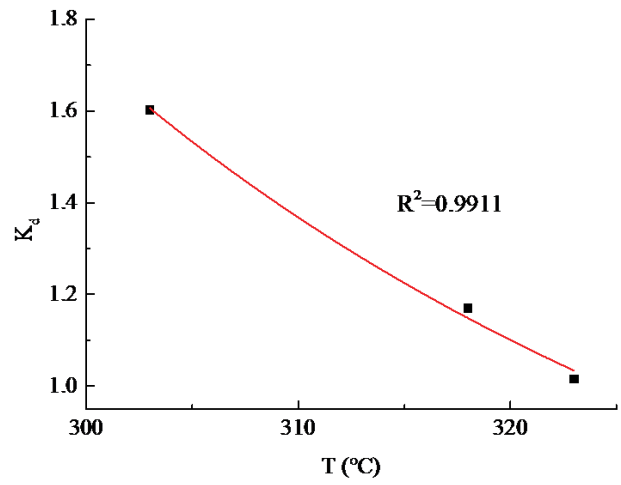


Fig. S3. Plot of K_d and T (303, 318, and 323 K).